# OPTICS DESIGN OPTIMIZATION FOR IBS DOMINATED BEAMS

F. Antoniou, H. Bartosik, Y. Papaphilippou, CERN, Geneva, Switzerland

N. Milas, A. Streun, Paul Scherrer Institut, Switzerland

M. Pivi, SLAC, Menlo Park, CA, USA

T. Demma, LAL, Université Paris-Sud, Orsay, France

## Abstract

Intra-beam scattering is a small angle multiple Coulomb scattering effect, leading to emittance growth. It becomes important for high brightness beams in low emittance lepton rings, but also hadron synchrotrons and ring colliders. Several theoretical models have been developed over the years, however, when the IBS becomes predominant, the divergence between the models becomes important. In addition, the theoretical models are based on the consideration of Gaussian beams and uncoupled transverse motion. Recently, two multi-particle tracking codes have been developed, in order to enable the understanding of the IBS influence on the beam distribution and the inclusion of coupling. The comparison between theoretical models in different lattices and different regimes is discussed here and the bench-marking of the theoretical models with the tracking codes is presented. Finally, first measurement results are presented in low emittance rings and hadron synchrotrons.

## INTRODUCTION

Future $e^+/e$ linear collider damping rings, b-factories, modern high brilliance light sources but also hadron synchrotrons and ring colliders, aim to produce high brightness beams, entering in a regime where collective effects and especially intra-beam scattering (IBS) are predominant.

IBS is a small angle multiple Coulomb scattering effect, which depends on the lattice and the beam characteristics, leading to the diffusion of the six-dimensional phase-space. Several theories and their approximations were developed over the years describing the effect. In this report, the theoretical models of Bjorken-Mtingwa (B-M) and Piwinski (P) and their high energy approximations, Bane and the Complete Integrated Modified Piwinski (CIMP) respectively are used [1–4].

One of the main weaknesses of all theoretical models is the consideration of Gaussian beam distributions whose preservation, especially in strong IBS regimes, is not evident. The generation of non-Gaussian tails and its impact on the damping process can only be investigated with multiparticle algorithms [5, 6]. The bench-marking of these theoretical and numerical models with beam experiments would be the ultimate goal for understanding IBS.

In this report, the IBS effect is studied for three different lattices at different regimes. The CLIC DRs for ultra low emittance beams, the SLS at low energy and high bunch current and the SPS for the ion beams. First measurement results are finally presented and discussed.

## IBS STUDIES FOR THE CLIC DR

The role of the CLIC DRs is to produce the required ultra low emittance at a high bunch intensity and a fast repetition rate, imposed by the luminosity requirements of the collider [7]. They have a racetrack configuration with two arc sections filled with theoretical minimum emittance (TME) cells and two long straight sections filled with superconducting wigglers, which are necessary for the fast damping and the ultra low emittance [7].

The CLIC DR have to deliver a high bunch intensity of $4.1 \times 10^9$ particles with ultra low horizontal and vertical emittances of 500 nm·rad and 5 nm·rad respectively, normalized to the beam energy. What indeed diversifies the required beam characteristics in the DRs is the very small longitudinal normalized emittance of 6 keV·m, which is imposed by the bunch compression requirements of the downstream RTML (Ring To Main Linac) system [7]. The increased beam density of the beam triggers a number of single bunch collective effects with Intrabeam Scattering (IBS) being the main limitation for the ultra low emittance.
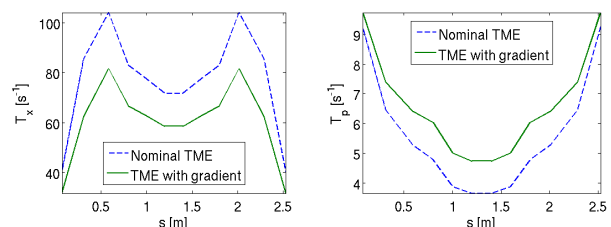


Figure 1: Horizontal (left) and longitudinal (right) growth rate increments along a nominal (blue-dashed) and a modified (solid-green) TME cell.

In the initial design of the CLIC DR [8] the nominal TME cells were used, targeting a very low equilibrium emittance. This was due to the fact that the IBS growth factor of the lattice at that stage of the design was very large ($\sim 6$). One of the first steps in the optimization procedure was to modify the TME cell, using a combined function dipole with a low defocusing gradient, calling this a modified TME cell. The low gradient do not have any impact on the emittance, however, it reverses the vertical beta function at the middle of the dipole, maximizing the vertical beam size at that location where all horizontal and vertical beam sizes and dispersion used to be minimum in the initial design [7]. This reduced the IBS growth factor by a factor of 2. Figure 1 shows the comparison of the horizontal (left) and longitudinal (right) IBS growth rate increments along a TME cell, for a nominal (dashed-blue lines) and a modified
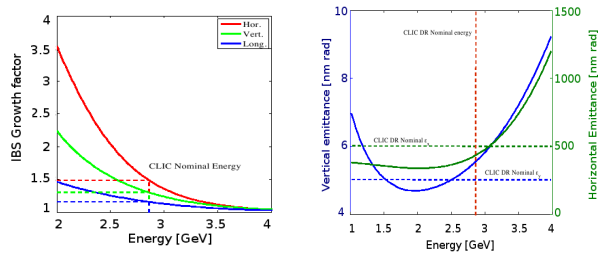
Figure 2: Scaling of the ratio between the steady state and zero current horizontal and vertical emittances with the energy (left). The dependence of the steady state emittances to the energy is shown in the right.

(solid-green lines) TME cell, calculated by the ibs module of madx [9]. In the example presented here, the IBS growth rates in the horizontal plane, where the effect is strong, are suppressed by 20 %.

In the CLIC baseline, a polarized electron and an unpolarized positron beams are considered. Therefore, the ring energy should be chosen so that the spin tune is a half integer to stay away from the strong integer spin resonances. The initial choice of energy was at 2.424 GeV. Several design and optimization steps where performed, however, even though focused in the minimization of the IBS effect, the emittance growth due to IBS was still a factor of 3. As the IBS growth rates but also the zero current equilibrium emittances depend on the energy of the beam, the scaling of the output emittance with the energy is studied. Figure 2 (left) shows the scaling of the ratio between the steady state and zero current horizontal and vertical emittances with the energy. The dependence of the steady state emittances to the energy is shown in Fig. 2 (right). A broad minimum is observed around 2.0 GeV for the horizontal and vertical emittances, where the IBS effect also becomes weaker. Although higher energies may be also interesting for reducing further collective effects, the output emittance is strongly increased due to the domination of quantum excitation. In this respect, it was decided to increase the DR complex energy from 2.424 GeV to 2.86 GeV. The new energy is close to a steady state emittance minimum but also reduces the IBS impact from 3 to 1.5 [10]. Reducing the IBS growth factor by a factor of 2, the requirement for the zero current horizontal emittance is also relaxed by a factor of 2. The number of wiggler magnets can then be reduced, reducing also the circumference of the ring.

## TME Optics Optimization with Respect to IBS

The Theoretical Minimum Emittance (TME) optics cells are the most compact configurations that can achieve the lowest possible emittance, for a unique high phase advance [11]. The strong focusing needed for accomplishing the TME conditions, results in intrinsically high chromaticity cells with reduced Dynamic Aperture (DA). An analytical solution for the quadrupole strengths and a complete parametrization of the TME cell, using thin lens approxi-
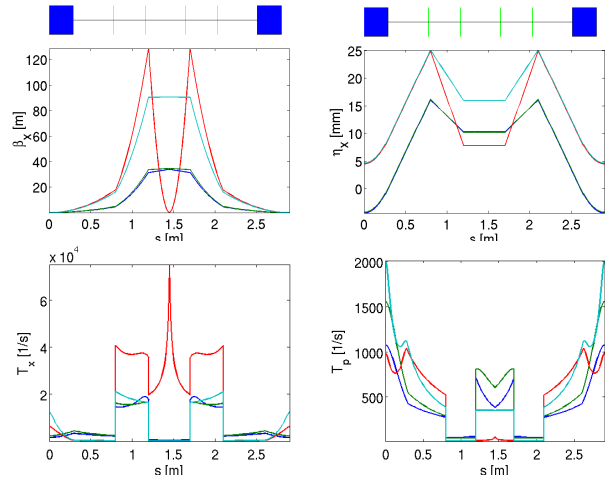


Figure 3: Different optics options for the same detuning factor (in this example DF=6) of a TME cell (top) and the respective horizontal (bottom, left) and longitudinal (bottom, right) growth rates.

mation, was developed, where, all cell properties, including the IBS growth rates, are globally determined and the optimization procedure following any design requirements can be performed in a systematic way [12].

An example of a cell with a dipole bending angle of $\theta = 2\pi/100$ and a dipole field of 1 T is used in the next to demonstrate the results. The calculations of the growth rates are done for a normalized horizontal emittance of $500 \text{ nm} \cdot \text{rad}$ and a vertical emittance of $5 \text{ nm} \cdot \text{rad}$.

The solutions for the horizontal beta function and dispersion of the TME cells, lie in different ellipses for different emittances or detuning factors (DF=$\epsilon_x/\epsilon_{\text{TME}}$). Thus, there are several optics options for each emittance, but only a few of them satisfy the stability criteria in both horizontal and vertical planes [12]. In Fig. 3 (top) three optics options are presented for the same detuning factor of the cell (DF=6). Figure 3 (bottom) shows the horizontal and longitudinal growth rates along the TME cell for those three different optics options, showing the dependence of the IBS growth rates on the optics of the machine.

Scanning in a large number of detuning factors (here from 1 to 25), one can find optimal regions of solutions according to the requirements of the design. Figure 4 shows the parametrization of the horizontal chromaticity (left) and the detuning factor (right) with the horizontal and vertical phase advances of the cell. In order to keep the chromaticity in low values, large detuning factors and small phase advances are needed. Figure 5 presents the parametrization of the mean horizontal (top, left) and mean longitudinal (top, right) growth rates and the Lasslet space charge tune shift with the horizontal and vertical phase advances of the cell, showing that in the same interesting region for the chromaticity minimization, the growth rates and the space charge tune shift are also optimal. For the case of the IBS growth rates, other phase advance solutions can minimize
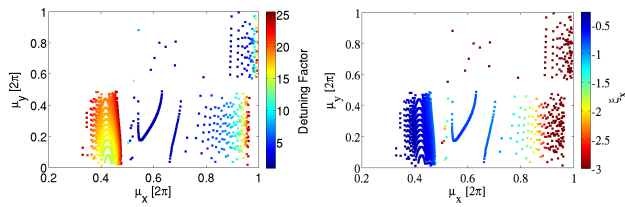
Figure 4: Parameterization of the cell detuning factor (left) and the horizontal chromaticity (right) with the horizontal and vertical phase advances of the TME cell.



Figure 6: SIRE (left) and CMAD-IBStrack (right) bench-marking with the theoretical models, for the one turn emittance evolution at the CLIC DR lattice.





Figure 7: Bench-marking of CMAD-IBStrack with Piwinski and Bane theoretical models, for the steady state horizontal (left) and longitudinal (right) emittances at the SLS lattice for three different current values: 1 mA (blue), 10 mA (red) and 17 mA (green).
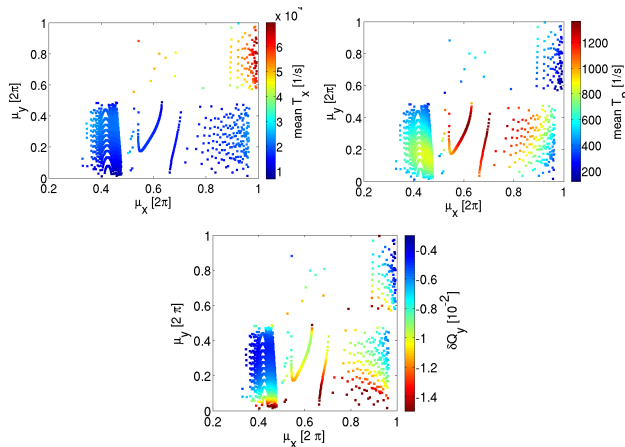
Figure 5: Parameterization of the horizontal (left) and longitudinal (right) IBS growth rates (top) and the Lasslet space charge tune shift (bottom) with the horizontal and vertical phase advances of the cell.

each growth rate indipentently but not both of them simultaneously. High horizontal and vertical phase advances can minimize the longitudinal growth rate, while the horizontal one gets maximized. High horizontal and small vertical phase advances minimize both the horizontal and longitudinal IBS growth rates, while the chromaticity and the space charge tune shift get maximized.

## IBS SIMULATION TOOLS

One of the main weaknesses of all IBS theoretical models is the consideration of Gaussian beam distributions, whose preservation, especially in the case of strong IBS, is not evident. The generation of non-Gaussian tails and its impact on the damping process can only be investigated with multiparticle algorithms. Another limitation, especially interesting for flat beams, is the consideration of uncoupled planes.

Recently, two multi-particle tracking codes were developed [5,6] which treat IBS, synchrotron radiation (SR) and quantum excitation (QE) regardless of the bunch distribution, giving the possibility to explore the generation of non-Gaussian tails and the effect of betatron coupling in the final beam distributions. The ultimate goal, is the bench-
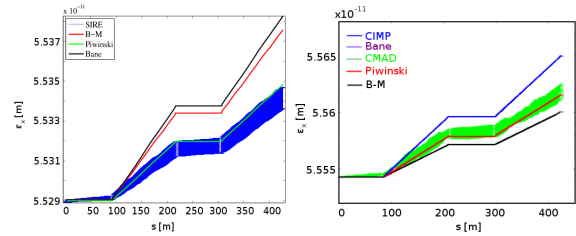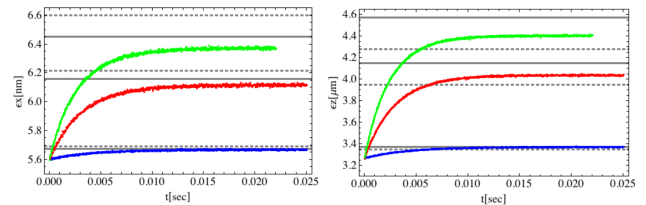
marking of the codes with the existing theoretical models and with IBS measurements for different machines at different IBS regimes.

A bench-marking of the SIRE [5] and CMAD-IBStrack [6] codes with the theoretical models [1–4], was performed for the CLIC DR lattice. Figure 6 shows the one turn comparison of the horizontal emittance evolution due to IBS for SIRE (left) and CMAD-IBStrack (right). For the tracking codes the $1\sigma$ error-bars are shown (blue for SIRE and green for CMAD-IBStrack). In both cases, there is a very good agreement between the tracking code and the Piwinski formalism. This is expected as the codes use the Rutherford cross section for the scattering, which is also used by Piwinski. Another interesting result, is that all theories and codes follow the same evolution trend around the ring. The main difference in those two examples is that in the first case, vertical dispersion is included, while for the second, zero vertical dispersion is considered.

The CMAD-IBStrack code was bench-marked for the SLS ring at nominal energy, for three different currents, 1 mA (blue), 10 mA (red) and 17 mA (green), thus different IBS regimes, with Bane (solid line) and Piwinski (dashed line). Figure 7 shows the horizontal (left) and longitudinal (right) emittance evolution in three damping times, where equilibrium has been reached. At 1 mA, where IBS is weak, there is perfect agreement between the theoretical models and the code. At higher currents, as the effect becomes more important, the divergence between the models and the codes becomes bigger.

## IBS MEASUREMENTS AT THE SLS

The Swiss Light Source (SLS) storage ring is an ideal test-bed for IBS experimental studies: a record vertical geometrical emittance of around 1 pm·rad at 2.4 GeV has been achieved [13], but also, the ring has the availability of emittance monitoring diagnostics and the ability to run at lower energies, where the IBS effect is strong.

In order to estimate the expected magnitude of the effect, the theoretical models of Piwinski, B-M, Bane and CIMP were used to calculate the IBS growth factor (ratio of the output emittance with IBS and the zero current emittance), for the nominal energy, En=2.4 GeV and a lower operational energy, En=1.6 GeV, showing that the effect is not visible at nominal energy while it can be strongly enhanced at low energy [14].

A first set of measurements at low energy was performed in May [14], where emittance growth with current had been observed. However, the longitudinal motion was dominated by the microwave instability (MI), making it very difficult to compare the measurements with the predictions from the IBS models, due to the luck of any MI model for the energy spread, while the beam size monitors are placed in a dispersive region [15].
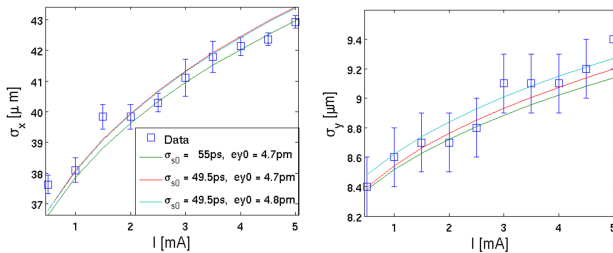


Figure 8: Horizontal (left) and vertical (right) beam size measurements for different bunch currents. The IBS predictions for different equilibrium bunch length and vertical emittance values are shown in solid lines.

A new set of measurements at low energy was performed in August 2012. The total current of the machine was kept always constant at 60-70 mA, in order to have enough light for the pinhole camera (horizontal beam size measurement) and to have the same effect from the $3^{rd}$ harmonic cavity. A different (random) filling pattern of the machine was used to change the bunch current, without triggering any multi-bunch instabilities.

Figure 8 shows the horizontal (left) and vertical (right) beam size measurements with current. Due to the effect of the third harmonic cavity, the bunch length was large, being out of the MI regime. The solid lines, show the IBS predictions for three different assumptions of the zero current bunch length and vertical emittance. The IBS calculations were done with the CIMP formalism. The results are very promising as the data seem to follow the IBS predicted behavior. However, more measurements are required in order to define correctly the zero current emittances, which is an input to the IBS calculations, and explore the phase space
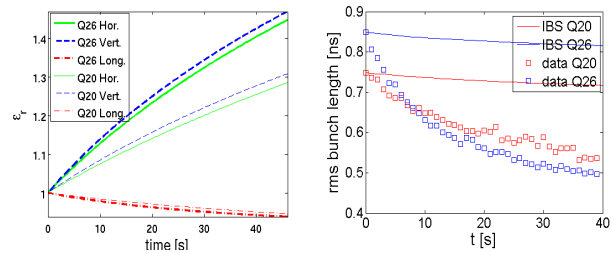


Figure 9: Left: IBS factor in the hor. (green-solid), vert. (blue-dashed) and long. (red-dashed-dotted) planes, for the Q20 (thin lines) and Q26 (thick lines) optics, for the same initial conditions. Right: Measured (squares) and IBS predicted (solid lines) bunch length evolution with time for the Q26 (blue) and the Q20 (red) optics.

in order to disentangle IBS from any other collective effects. Comparison with the tracking codes is also foreseen.

## IBS OBSERVATIONS IN THE ION BEAMS AT THE SPS

During the setting up of the ion beams at the SPS, a spread on the parameters of the lead ion beam bunches, at flat top, was observed. Even though this is not a limitation for the performance of the LHC as lead ion collider, it would be interesting to try to overcome this bunch parameter spread, which is mainly dominated by processes at the flat bottom of the SPS [16]. As the Q20 optics appear to improve the performance of the SPS for the proton beams [17], it was proposed to be used as an alternative for the ion beams too for reducing scattering effects and space charge, due to larger beam sizes.

Figure 9 (left) shows a comparison of the IBS effect for the nominal Q26 (thick lines) and the Q20 (thin lines) optics in the horizontal (green-solid), vertical (blue-dashed) and longitudinal (red-dashed-dotted) planes, for the same initial conditions and for the same current. The Piwinski formalism was used for the calculation of the IBS growth rates and the emittances' evolution with time, for a cycle duration of 40 sec. In both cases transverse emittance growth and longitudinal emittance damping with time is predicted. The effect in the transverse plane is $\sim 15\%$ larger in the Q26 than the Q20 optics, while in the longitudinal plane the effect is almost the same. Figure 9 (right) shows the measured bunch length evolution with time for Q26 (blue, squares) and Q20 (red, squares) optics. Using as initial bunch length the measured one, the bunch length evolution due to IBS was computed for the measured current. The results are shown in solid lines in blue for the Q26 and in red for the Q20 optics. Even though IBS predicts bunch shortening, the effect predicted by IBS is much smaller than the observed one.

In the large scattering angle limit of the coulomb scattering, the Touschek effect leads to beam losses due to large exchange of momentum between the colliding particles.

The non-relativistic round beam approach of the touschek lifetime can be found in [18].

Assuming a general quadratic form for the current decay with time of the form:

$$\frac{dI}{dt} = -\frac{I}{b} - \frac{I^2}{a} \tag{1}$$

the time depended current expression is given by:

$$I(t) = \frac{\alpha I_0 e^{-t/b}}{b I_0 (1 - e^{-t/b}) + \alpha} \tag{2}$$

Comparing eq. (1) with the Touschek lifetime expression, the parameter $\alpha$, called the Touschek parameter, can be written as:

$$\alpha = \frac{e n_e 8 \sqrt{\pi} \beta_r^2 \gamma^4 \sigma_z \sigma_p \epsilon_x \epsilon_y}{r_e^2 c T_0 \langle \sigma_H F(\tau_m) \rangle} \tag{3}$$

$\tau_m \equiv \delta_{acc}^2 = \frac{2n_e V_{rf}}{\pi h \eta_p \beta_r^2 E n}$, where, $\delta_{acc}$ is the minimum acceptance of the machine (i.e. RF momentum acceptance or dynamic acceptance). For the case of the SPS, the minimum acceptance is the RF momentum acceptance. The parameter b, corresponds to the lifetime factor due to other effects.

In order to calculate the expected current decay with time due to the Touschek effect, the Touschek parameter is calculated for each measured bunch length, considering the horizontal and vertical emittances unchanged. As the acceptance is not a well known parameter, and the calculations are very sensitive to this, the calculations are performed for different acceptance values, assuming as a first approximation, that this is a constant around the ring. The expected current decay with time can then be calculated from eq. (2), while the b parameter needs to be defined.

Figure 10 shows the measured current decay with time (blue squares) while the solid lines show the expected decay with time based on the above calculations, for different values of the b factor. For the Q26 optics (left), there is no b factor for which a "Touschek like" behavior applies to all data. However, considering fast losses in the beginning due to other effects (e.g. space charge), which are not linear with time and cannot be included in the b factor, the data seem to follow a "Touschek like" behavior. On the other hand, the data from the Q20 optics (right), seem to follow a "Touschek like" behavior from the beginning.

As the analysis is still in a preliminary stage, what can be stated for now is that a nonlinear, quadratic, term is needed to describe the current decay of the ion beams at the SPS. For both cases, the theoretical curves for $\delta_{acc} = 0.9\%$ fit better with the data.

## CONCLUSION AND OUTLOOK

Intrabeam scattering is an effect which becomes important in high brightness synchrotrons and becomes a limiting factor for their performance. Systematic optics optimization is very important for the mitigation of the effect.
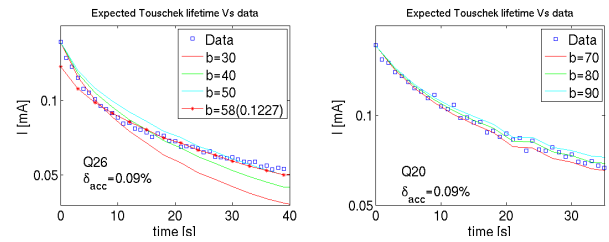
Figure 10: Measured (blue squares) and expected Touschek (solid lines) current decay with time for the Q26 (left) and Q20 (right) optics.

The existing IBS theoretical models, considering Gaussian beam distributions and uncoupled frames, cannot study interesting aspects of IBS like the impact on the final beam distribution and on the damping process. For this, the development of multiparticle tracking algorithms is essential. The ultimate goal is the bench-marking of the tracking codes with the theoretical models and with beam data, at different machines and different regimes of the effect.

## ACKNOWLEDGEMENTS

## REFERENCES

[1] J. Bjorken and S. Mtingwa, Part. Accel., v13, p115, 1983.

[2] A. Piwinski, Proc. 9th International Conference of High Energy Accelerators, Standford, CA, p.405, 1974.

[3] K. Bane, Proc. EPAC2002, Paris, France, p.1443.

[4] K. Kubo, et al., PRST-AB 8, 081001, 2005.

[5] A. Vivoli, M. Martini, Proc. IPAC2010, Kyoto, Japan.

[6] T. Demma et al, Proc. IPAC2011, San Sebastian, p.2259.

[7] CLIC Conseptual Design Report, preprint.

[8] M.Korostelev, PhD Thesis, CERN, 2006

[9] "MAD - Methodical Accelerator Design", available at the URL: http://mad.web.cern.ch/mad/

[10] F. Antoniou, M. Martini, Y. Papaphilippou and A. Vivoli, WEPW085, IPAC2010, Kyoto.

[11] A. Streun., CERN-2006-002, pp. 217-244, 2006.

[12] F. Antoniou, PhD Thesis, preprint.

[13] M. Aiba, et al., preprint.

[14] F. Antoniou et al, proc. of IPAC12, New Orleans, 2012, TUPPR057.

[15] N. Milas et al, proc. of IPAC12, New Orleans, 2012, TUPPC034.

[16] T. Bohl, Note 2011-72, CERN, Geneva, November 2011.

[17] F. Antoniou et al, proc. of IPAC12, New Orleans, 2012, WEPPR072.

[18] A. Piwinski, arXiv:physics/9903034.